Received: 19 June 2020 | Revised: 11 March 2021 | Accepted: 28 March 2021

DOI: 10.1002/hipo.23331

RESEARCH ARTICLE

WILEY

Object and object-memory representations across the proximodistal axis of CA1

Brianna Vandrey[1,2] | Stephen Duncan[1] | James A. Ainge[1]

[1]University of St Andrews, School of Psychology and Neuroscience, St Andrews, Fife, UK

[2]University of Edinburgh, Centre for Discovery Brain Sciences, Edinburgh, EH8 9XD, UK

Correspondence
James A. Ainge, University of St Andrews, School of Psychology and Neuroscience, St Andrews, Fife KY16 9AZ, UK.
Email: jaa7@st-andrews.ac.uk

Funding information
Royal Society of Edinburgh

Abstract

Episodic memory requires information about objects to be integrated into a spatial framework. Place cells in the hippocampus encode spatial representations of objects that could be generated through signaling from the entorhinal cortex. Projections from lateral (LEC) and medial entorhinal cortex (MEC) to the hippocampus terminate in distal and proximal CA1, respectively. We recorded place cells in distal and proximal CA1 as rats explored an environment that contained objects. Place cells in distal CA1 demonstrated higher measures of spatial tuning, stability, and closer proximity of place fields to objects. Furthermore, remapping to object displacement was modulated by place field proximity to objects in distal, but not proximal CA1. Finally, representations of previous object locations were closer to those locations in distal CA1 than proximal CA1. Our data suggest that in cue-rich environments, LEC inputs to the hippocampus support spatial representations with higher spatial tuning, closer proximity to objects, and greater stability than those receiving inputs from MEC. This is consistent with functional segregation in the entorhinal–hippocampal circuits underlying object-place memory.

KEYWORDS
CA1 region, entorhinal cortex, episodic memory, hippocampus, place cell, spatial memory

1 | INTRODUCTION

Episodic memory is memory for past personal experiences. Models of the neural circuits underlying episodic memory suggest that spatial input from medial entorhinal cortex (MEC) is combined with non-spatial item information from lateral entorhinal cortex (LEC) to form context-dependent memories within the hippocampus (Ainge et al., 2012; Ainge, Tamosiunaite, et al., 2007; Ainge, van der Meer, et al., 2007; Eichenbaum et al., 2012; Ferbinteanu & Shapiro, 2003; Hayman & Jeffery, 2008; Leutgeb et al., 2005; Manns & Eichenbaum, 2006). Consistent with this, place cells in the hippocampus encode spatial representations of current and previous object locations (Deshmukh & Knierim, 2013; O'Keefe, 1976) that could be generated by signaling from entorhinal cortex (EC) (Deshmukh & Knierim, 2011; Høydal et al., 2019; Tsao et al., 2013; Tsao et al., 2018; Wang et al., 2018).

Manipulation studies demonstrate that memory for objects within specific locations is dependent on both EC and hippocampus (Aggleton & Nelson, 2020). However, object-location memory can be tested in different ways. In complex tests, multiple objects are presented in different locations and object-location memory is tested by moving and/or replacing them with different objects. Simpler tasks present only two objects and object-location memory is tested by moving or replacing one object to create a new configuration of object and location. Lesions of the hippocampus impair all forms of object-location memory (Barker et al., 2017; Barker & Warburton, 2011; Mumby

et al., 2002; Save et al., 1992; Warburton & Brown, 2010, although see Eacott & Norman, 2004; Langston & Wood, 2010). Manipulations of EC, however, produce a more nuanced deficit. Complete MEC lesions produce deficits in recognizing that a familiar object has moved to a novel location (Rodo et al., 2017; Van Cauter et al., 2013) and specific inactivation of stellate cells in the superficial MEC has a similar effect (Tennant et al., 2018). In contrast, lesions of LEC impair the ability to remember specific object-location associations (Wilson, Langston, et al., 2013). Object-location memory deficits are more pronounced in both MEC and LEC lesioned animals in more complex tasks that require memory for multiple object-location associations (Kuruvilla & Ainge, 2017; Rodo et al., 2017). These observations demonstrate that the entorhinal–hippocampal network is critical for associating objects with the locations in which they were experienced, and suggests functionally segregated subsystems within the network that integrate object and location information in different ways.

Functional segregation within the entorhinal–hippocampal network is consistent with its anatomy. Inputs from EC are partially segregated in the hippocampus, and projections from LEC and MEC terminate in distinct regions of the CA1 proximodistal axis. LEC sends projections predominantly to distal CA1, bordering the subiculum, while MEC projects predominantly to proximal CA1, bordering CA2 (Masurkar et al., 2017; Michael Wyss, 1981; Naber et al., 2001; Steward, 1976; Tamamaki & Nojyo, 1995; Witter et al., 2000). Examination of how objects are represented in LEC and MEC also suggests segregated functional networks (Deshmukh & Knierim, 2011, 2013; Høydal et al., 2019; Tsao et al., 2013, 2018). LEC contains cells that develop specific and consistent spatial signals in the presence of objects (Deshmukh & Knierim, 2011, 2013; Tsao et al., 2013, 2018). A subset of these neurons also generate responses to empty positions in which objects have previously been experienced, suggesting a neural correlate for object-location memory (Tsao et al., 2013, 2018). In comparison, a significant proportion of MEC cells encode vector relationships between objects and the position of the animal (Høydal et al., 2019). This is consistent with the suggestion that different types of responses to objects are maintained in functionally separate entorhinal–hippocampal circuits. Further support for this suggestion comes from studies showing distal CA1 is preferentially recruited to process information about objects (Hartzell et al., 2013; Ito & Schuman, 2012; Nakamura et al., 2013; Nakazawa et al., 2016), and place cells in proximal CA1 demonstrate higher spatial tuning and stability than place cells in distal CA1 in empty environments (Henriksen et al., 2010). However, it is unclear whether differences across the proximodistal axis of CA1 persist in cue-rich environments.

We examined whether place cells in distal and proximal CA1 are differentially modulated by the presence of objects, and whether EC inputs influence the spatial representation of objects in CA1. We recorded place cell activity as rats foraged in an environment that contained objects. We report higher measures of spatial tuning in distal CA1, which receives LEC inputs, in comparison to proximal CA1, which receives MEC inputs. Spatial representations were more stable in distal CA1 than proximal CA1 and this stability was modulated by proximity to objects in distal CA1. Furthermore, place fields generated in distal CA1 were closer to objects and locations where objects were previously experienced.

2 | MATERIALS AND METHODS

2.1 | Animals

Animals were adult male Lister-hooded rats (n = 7) weighing 330–450 g at the time of surgery. Prior to surgery, animals were housed in groups of 2–4 in diurnal light conditions (12-h light/dark cycle). After surgery, animals were housed individually. All habituation and testing occurred during the light phase. Animals had ad libitum access to water throughout the study. To encourage exploration during the behavioral task, animals were food deprived to ≥90% of their free-feeding weight. All experiments were conducted under a project license (70/8306) acquired from the UK home office and in accordance with national (Animal [Scientific Procedures] Act, 1986) and international (European Communities Council Directive 2010; 2010/63/EU) legislation governing the use of laboratory animals in scientific research.

2.2 | Surgical implantation of electrodes

Microdrives contained four tetrodes, each comprising four electrodes. Tetrodes were constructed by twisting together 17 μm platinum-iridium wire. Tetrodes were threaded through a 20-gauge steel cannula, which was secured to the microdrive with dental cement. Each microdrive was fitted with a built-in groundwire and a screw mechanism which could be turned to lower the electrodes vertically into the brain. Before implantation, tetrodes were plated with gold to lower the impedance of the electrode tip to 200–300 kΩ. For surgical implantation of the electrodes, rats were anaesthetized with isoflurane before being transferred to a stereotaxic frame. The rats were administered an analgesic (Carprofen) subcutaneously prior to incision. The skull was exposed, and the microdrives were implanted aimed at distal (n = 4 animals) or proximal CA1 (n = 2 animals). Where implants were bilateral (n = 1 animal), one microdrive was aimed at each region of CA1. Coordinates for distal CA1 were 5.0 posterior to bregma and 3.2 lateral to midline. Coordinates for proximal CA1 were 3.6 mm posterior to bregma and 3.8 mm lateral to midline. For each implant, a craniotomy was made at the relevant coordinates, dura was cut, and the electrode was lowered vertically 1.8 mm from the surface of the brain. Implants were secured to the skull using a combination of jewellers screws and dental cement. The groundwire of each microdrive was secured to a screw near the front of the skull. Animals were administered oral analgesic (Metacam) in their diet for 3 days postsurgery.

2.3 | Recording

Screening for units commenced within 1 week after surgery. A recording cable was connected to the microdrive which relayed unfiltered

electrical signals from each tetrode to the digital acquisition system (AXONA Ltd, UK). Signals were amplified with a unity-gain operational amplifier, and passed through a preamplifier. The signal was bandpass filtered (600–6,000 Hz) and amplified (5000–20,000 times). To screen for units, the filtered electrical signal for each tetrode was examined for spiking events via an oscilloscope on a computer screen. Furthermore, population-level EEG signal was examined for frequency characteristics of the hippocampus (theta; 8–12 Hz) to infer the position of each electrode in the brain. If no units were detected, electrodes were lowered vertically into the brain at small increments (≥50 μm). To record neuronal activity, each channel was monitored and 50 samples of 20 μs were collected per channel whenever the signal on any one of the four channels of a tetrode exceeded a predetermined threshold that was set based on the signal to noise ratio.

2.4 | Behavioral apparatus

The electrophysiology suite included a screening location (a pot lined with a towel) and a test environment. The test environment was a square wooden box (60 cm × 60 cm × 90 cm), with a white floor and black and white vertically striped walls. To secure objects in place within the test environment, square sections of fastening tape were attached to the middle of each quadrant of the box floor. This experiment used an array of junk objects which were approximately the same size as a rat and varied in color, shape, and texture. Any object used in habituation was not recycled during testing. During behavioral sessions, identical copies of each object were presented across trials. The same copy of each object was used across standard trials. Objects were cleaned thoroughly with veterinary disinfectant before each trial. Different objects were used on each day of testing. A local cue (colored cardboard) was attached to the wall of the upper right quadrant, and stable global cues in the room (e.g., lamps) were visible to the animal throughout testing.

2.5 | Habituation

Animals were habituated to the electrophysiology suite over five consecutive days prior to surgery. On each day of habituation, each animal was placed in the screening location individually for 10 min before exposure to the test environment. On Day 1, each animal explored the test environment with their cagemates for 10 min. On Days 2–5, each animal explored the test environment individually for 10 min. On Day 5, two identical objects were introduced in the test environment at the locations occupied by objects in the standard trials of the behavioral task. For all trials, the animal was placed in the test environment facing away from the objects.

2.6 | Behavioral task

A behavioral session consisted of five consecutive trials, including two object manipulations bounded by standard trials where the objects were presented in a familiar configuration. In the first trial, the animal encountered two different novel objects in the bottom left and right quadrants of the test environment (Standard Trial 1, S1). In the subsequent trial, the animal encountered a copy of each of the objects from the standard trials, but one was moved to a novel location in the upper left or right quadrant of the environment (Object Displacement, O1). The third trial was a repetition of the standard trial (Standard Trial 2, S2). In the fourth trial, the animal encountered two copies of one object from the standard trial in the bottom right and left quadrants of the test environment. One copy was in a novel configuration of object and location, and one copy was in a familiar configuration (Object-Place Recognition, O2). The final trial was a repetition of the standard trial (Standard Trial 3, S3). Each trial was 8 min long. The animal rested in the screening location for 5 min between trials. The environment was cleaned with veterinary disinfectant between trials to remove waste and neutralize olfactory cues. Across days, the side on which the object manipulation occurred (left or right) was counterbalanced to be pseudorandom. Video footage of the first 3 min of exploration was recorded by a camera positioned above the environment. After 3 min elapsed, food pellets (Dustless Precision Pellets, 45 mg, BioServ) were scattered randomly throughout the box to encourage exploration of the entire environment.

2.7 | Histology

Animals were administered a lethal dose of sodium pentobarbital and transcardially perfused with phosphate-buffered saline (PBS), followed by 300 mL paraformaldehyde (PFA, 4%). To increase the visibility of the electrode tract, the brain was stored within the skull for 24 h at 4°C. Brains were then extracted and stored in a 20% sucrose solution prepared in PBS for a minimum of 24 h at 4°C. The brain was sectioned coronally at 50 μm on a freezing microtome. 1:4 sections were mounted on slides and fixed for a minimum of 1 h in a PFA bath. To counterstain cell bodies, sections were defatted with xylene, and rehydrated by briefly immersing the slides in a series of ethanol solutions: 100% ethanol, 50% ethanol solution prepared in distilled water (dH_2O), and then in dH_2O. Slides were then immersed in a cresyl violet solution for 2 min, and washed in running tap water for 5 min. Sections were then dehydrated by briefly immersing the slides in the ethanol solutions in reverse order: dH_2O, 50% ethanol in dH_2O, and then 100% ethanol. Sections were then cover-slipped with DPX mountant. To confirm the location of the electrode tracts, slides were examined at a 4× magnification using a light microscope (Leitz Diaplan).

2.8 | Behavioral analysis

Behavioral footage was scored offline. The amount of time spent exploring each object was measured in seconds for all trials. To determine whether the animal preferentially explored the object in a novel spatial configuration, a discrimination ratio was calculated for each object manipulation using the following formula (Ennaceur & Delacour, 1988):

$$\text{Discrimination ratio} = \frac{(\text{Exploration novel(s)} - \text{Exploration familiar(s)})}{\text{Total exploration time (s)}}$$

The discrimination ratio is calculated by subtracting the amount of time spent exploring the object in the familiar configuration from the amount of time spent exploring the object in the novel configuration, and then dividing this value by the total exploration time. A positive value indicates an exploratory preference for the object in a novel configuration. For each animal, average discrimination ratios were calculated for each object manipulation. Population means and standard errors of the mean were calculated from these averages. Discrimination ratios are calculated from the first 3 min of each trial.

2.9 | Place cell identification

Single units were isolated from the raw data using TINT (AXONA Ltd). First, spike clusters were generated using an automated clustering software, KlustaKwik, which clusters spikes using principal components. Clusters which did not resemble neuronal spikes were removed. The remaining clusters were manually refined by comparing peak amplitude, trough, and time-to-peak and trough on each channel. Only units with a minimum of one place field in any trial of a session, a spatial information score of ≥0.5 in all trials where the unit expressed a place field, an average firing rate between 0.1 and 2.5 Hz, and a mean spike duration of ≥250 ms were accepted for analysis. To detect place fields for each unit, the position data was sorted into 2 × 2 cm bins. Place fields were defined as contiguous regions of ≥6 bins where the firing rate was ≥20% of the peak firing rate for that unit during the trial. Finally, putative place cells were screened using a shuffling procedure to guard against spurious bursts of activity causing high spatial information in low firing rate cells. A randomized distribution of information scores was calculated for each putative place cell by shuffling their spike times relative to their corresponding spike positions. Spike times were shifted by a random length of time no less than 30 s. Through this method, 1,000 randomized rate maps were produced for each cell and information scores were calculated for each of them. The threshold for place cell definition was set at the 99th percentile of this randomized distribution of information scores.

2.10 | Quantification of cluster quality

To quantify the quality of each cluster, the isolation distance was calculated as described previously (Schmitzer-Torbert et al., 2005). For each cluster *c* with *n* spikes, isolation distance is defined as the squared Mahalanobis distance of the *n*th closest non-*c* spike to the center of the cluster. The squared Mahalanobis distance was calculated as:

$$D^2_{i,C} = (X_i - \mu_c)^T \sum_c^{-1} (X_i - \mu_c)$$

where x_i is a vector containing feature for spike *i*, and μ_c is the main feature vector for cluster *c*. High values indicate better isolation. Units with an isolation distance ≥20 were classified as highly isolated, units with an isolation distance ≥10 but <20 were classified as intermediately isolated, and units with an isolation distance <10 were classified as poorly isolated. The calculation of isolation distances required a good connection on all channels of a tetrode. When a channel was grounded due to noise or disconnection, cluster quality was manually categorized as high, intermediate, or poor by visual comparison against clusters for which an isolation distance value could be determined. When the same unit was recorded across multiple consecutive days, the recording with the highest average spatial information score was included in the analysis, and other recordings of this unit were discarded. Repeat recordings were determined by examining the shape of the waveform, the tetrodes on which it was recorded, and location of the place field(s).

2.11 | Analysis of place cell characteristics

Isolated units were processed offline using customized MATLAB scripts. Rate maps were generated by dividing the area of the box into pixels corresponding to 2 × 2 cm bins of the environment. The firing rate in each pixel was determined by dividing the number of spikes by the dwell-time of the animal in that bin. Firing rate maps depict the firing rate of each bin in color, where blue represents the lowest firing rate and red represents the highest firing rate. The firing rate maps were analyzed from the whole 8 min trial to extract the following characteristics: spatial information content, selectivity, spatial coherence, average firing rate, peak firing rate, place field frequency, and place field size.

The spatial information content of a unit, presented as a ratio of bits/spike, indicates the amount of information about the location of an animal which is encoded in each spike. This was calculated using the following formula (Skaggs et al., 1993):

$$\text{Spatial information content} = \sum\nolimits_i P_i \frac{\lambda_i}{\lambda} \log_2 \frac{\lambda_i}{\lambda}$$

where λ_i is the average firing rate of a unit in the *i*th bin, λ is the overall average firing rate, and p_i is the probability of the animal being in the *i*th bin (dwell time in the *i*th bin/total recording time). The average firing rate was calculated by dividing the total number of spikes in a trial by the trial duration, and the peak firing rate was the maximum firing rate within the firing field(s) of the cell. Selectivity is a measure of how specific the spikes from the cell are to the place field(s) in an environment and was calculated by dividing the maximum firing rate by the average firing rate. Spatial coherence estimates how coherent a firing field is by determining the extent to which firing rates within a pixel are matched with firing rates in adjacent pixels. This measure is calculated by correlating firing rates within each pixel with the firing rates in eight adjacent pixels, and returning the z-transform of this correlation (Muller & Kubie, 1987). To determine the stability of rate maps across trials, each pixel of the rate map from one trial was correlated with the corresponding pixel from a rate map from a second trial, generating a Pearson's correlation coefficient. Pixels corresponding to

locations in the environment which the animal did not visit in either trial were discarded.

2.12 | Analysis of place fields

To examine the location of place fields across the environment, the area of the test environment was divided into 8 × 8 bins and the coordinates assigned to the centroid of each place field were plotted across these bins. The centroid of a place field was defined as the average position of the pixels of a place field along the X and Y axis, weighted by the firing rate of those pixels. Using this division of the environment, each quadrant of the environment constituted an array of 16 bins, where the four central bins (15 × 15 cm) correspond to the location of the object in each quadrant and the outer 12 bins correspond to locations around the object within the quadrant. Frequencies of place fields in each quadrant, and at previous and current object locations were extracted using these criteria. To determine the distance of place fields from objects in the environment, the Euclidean distance between the object centroid, defined as the center of the object quadrant, and the place field centroid, was measured.

2.13 | Analysis of remapping and trace firing

Population changes in spatial coding were quantified by examining the correlation of rate maps across trials. Remapping of individual cells in response to object displacement was quantified by examining the location of place field centroids and correlation of rate maps across S1, O1, and S2. Any cell which expressed no field in S1 and O1 or had a correlation coefficient between S1 and O1 which was greater than or equal to the average correlation coefficient between S1 and S2 for that region (distal or proximal) was categorized as nonremapping. The place fields of the remaining cells were examined for patterns corresponding to remapping behaviors that have been described previously (Deshmukh & Knierim, 2013; Lenck-Santini et al., 2005; Manns & Eichenbaum, 2009; Muller & Kubie, 1987). Place cells were categorized as remapping if they expressed a place field in the novel object quadrant in O1, but not S1, or the peak firing rate within a pre-existing place field in the novel object quadrant was reduced ≥25% in O1. Place cells were also categorized as remapping if a new place field appeared at any location in the environment, if the number of place fields reduced between S1 and O1, or if a pre-existing place field shifted ≥7.5 cm. A cutoff value of 7.5 cm was chosen given that this distance corresponds with the widths of the bins used to generate the plots of centroid locations. Remapping of place field locations was not examined for the novel object-place recognition trial given that the literature does not predict remapping to this type of manipulation (Deshmukh & Knierim, 2013; Lenck-Santini et al., 2005; Manns & Eichenbaum, 2009).

To quantify rate remapping in response to a change in object identity, firing rate changes were calculated as the normalized rate differences between the first standard trial and the object-place recognition trial (O2) and the second standard trial and O2. These values were calculated by taking the absolute value of the difference in firing rate between the two trials, divided by the sum of the firing rates across the two trials (Lu et al., 2013).

Trace firing was quantified by examining the location of place field centroids across S1, O1, and S2. Place cells were categorized as "misplace" cells if they expressed a place field in the empty quadrant which previously contained the displaced object in O1, but not S1 (O'Keefe, 1976). Place cells were categorized as remap "trace" cells if they expressed a place field in the quadrant which contained the displaced object in O1, but not S1, and a place field persisted in this quadrant in S2. Place cells were categorized as nonremap "trace" cells if they did not express a place field in the quadrant which contained the displaced object in S1 or O1 but did express a place field in this quadrant in S2.

2.14 | Statistical analyses

All statistics were calculated using R (www.R-project.org). To determine whether there was a significant difference across groups for behavior, univariate ANOVAs were conducted with region (proximal vs. distal) as a between-subjects factor. For place cell characteristics and vector distances, mixed factorial ANOVAs were conducted with region (proximal vs. distal) and trial (S1 vs. S2 vs. S3 vs. O1 vs. O2) as factors. Post hoc comparisons were performed using Tukey's Honest Significant Difference test. Stability of place cell representations across sessions was calculated using Pearson's correlations. To determine whether patterns of remapping or trace firing in response to changes in the position of objects were observed at similar proportions across groups, observed frequencies were compared across proximal and distal CA1 using a Chi-square test of independence.

3 | RESULTS

We recorded from place cells in distal and proximal CA1 (1,415 place fields across all trials [distal n = 1,158, proximal n = 257] from 249 units [distal n = 208, 5 animals; proximal n = 41, 3 animals]) as rats foraged in a square environment containing two different objects (Figure 1a,b; Table S1). Place cell characteristics were compared across standard trials (S1–S3) where object locations were consistent and manipulation trials where either the location (O1) or identity (O2) of one object was manipulated. The time spent exploring the object in a novel configuration was measured in each manipulation trial to confirm recognition of the spatial change (Figure S1). Cluster qualities were similar across distal and proximal CA1 (Figure S2; highly isolated, distal: 111/208 cells, 53.4%; proximal: 21/41 cells, 51.2%; intermediately isolated: distal: 97/208 cells, 46.6%; proximal: 20/41 cells, 48.8%; χ^2 (1) = 0.0633, p = .801334).

We first asked whether the increased spatial tuning in proximal CA1 relative to distal CA1 reported in empty environments (Henriksen et al., 2010) persists in an environment that contains

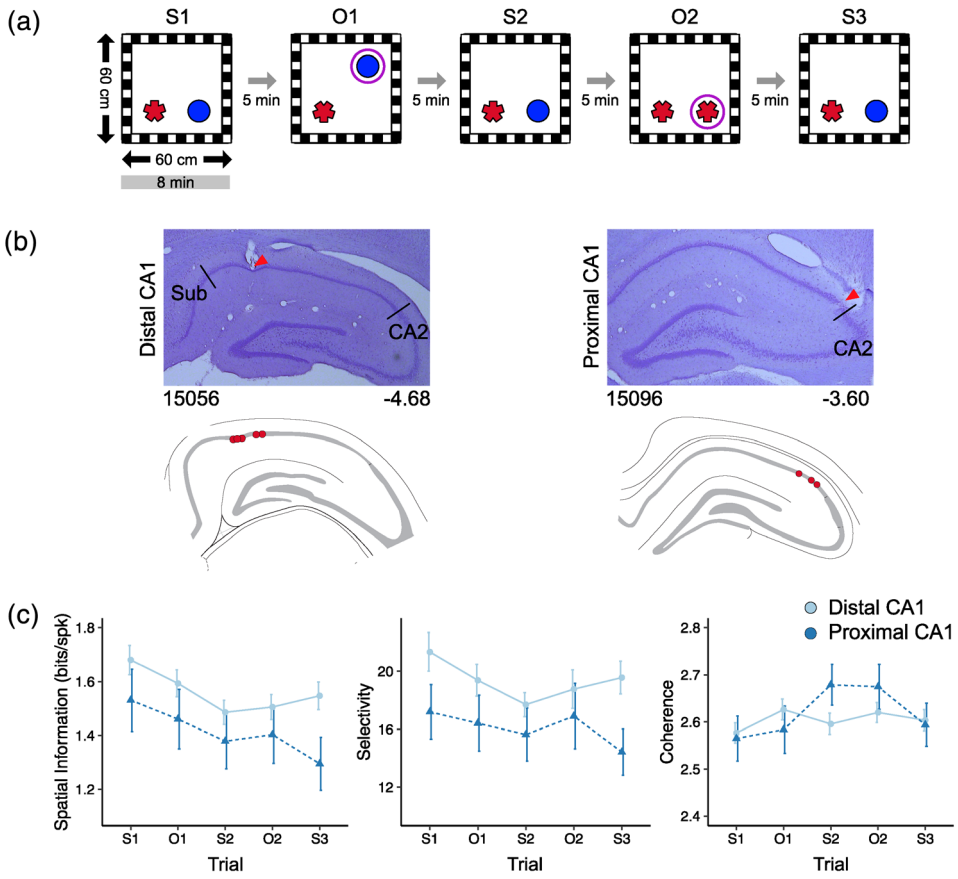

FIGURE 1 Spatial tuning across the proximodistal axis of CA1. (a) Schematic of test trials. Each test session consisted of three standard trials (S1–S3) interleaved with two manipulation trials where an object was displaced to a novel location (O1) or appeared in a novel object-place configuration (O2). Circles indicate the novel configuration in the manipulation trials. (b) Representative examples of electrode tracts in distal (left) and proximal CA1 (right) in coronal sections of tissue stained with cresyl violet. Red arrow indicates tract location. Numbers indicate animal (left) and caudal distance from bregma (right). Schematic beneath each image shows electrode tract locations for all animals in each group. Each red dot indicates a single animal. (c) Line plots comparing spatial information (left), selectivity (middle), and spatial coherence (right) across trials for place cells in distal (light blue, solid line) and proximal CA1 (dark blue, dashed line). Markers (distal = circle, proximal = triangle) represent mean values for each trial. Error bars are SEM [Color figure can be viewed at wileyonlinelibrary.com]

objects (Figure 1c). Spatial information in distal CA1 was found to be consistently higher than in proximal CA1, confirmed by a significant main effect of CA1 region ($F_{(1,1197)}$ = 7.229, p = .007) and no trial × region interaction ($F_{(4,1197)}$ = 0.234, p = .919) in a mixed factorial ANOVA. There was also a significant main effect of trial ($F_{(4,1197)}$ = 2.921, p = .020), and post hoc pairwise comparisons revealed significantly higher spatial information in the first standard trial than in the second standard trial (p = .024), with no other significant comparisons. These results demonstrate that distal CA1 place cells had consistently higher levels of spatial tuning across the experiment. A similar pattern was found for selectivity with distal CA1 place fields being more selective than proximal CA1, confirmed by a significant main effect of region ($F_{(1,1197)}$ = 6.783, p = .009) with no main effect of trial ($F_{(4,1197)}$ = 1.400, p = .232) or trial × region interaction ($F_{(4,1197)}$ = 0.248, p = .919). No differences were found in spatial coherence across region ($F_{(4,1197)}$ = 0.389, p = .533) or trial ($F_{(4,1197)}$ = 1.089, p = .360) and there was no trial × region interaction ($F_{(4,1197)}$ = 0.212, p = .645). These findings contrast previous reports of higher spatial tuning in proximal CA1, which receives inputs from MEC, in environments devoid of local cues (Henriksen et al., 2010). Our data demonstrate that in environments containing prominent local landmarks spatial tuning is higher in CA1 place cells that receive inputs from LEC relative to those receiving input from MEC.

Place cells in distal CA1 express more place fields than place cells in proximal CA1 in an empty environment (Henriksen et al., 2010). However, objects modulate the size and frequency of place fields in distal CA1 (Burke et al., 2011), indicating that a different pattern of place field expression could emerge in our environment. Place cells in proximal CA1 expressed more place fields than place cells in distal CA1 (Figure 2a; distal $\bar{x}$ = 1.14 ± 0.74 fields, proximal $\bar{x}$ = 1.28 ± 0.76 fields, $F_{(1,1195)}$ = 5.876, p = .016), but the size of place fields was similar across the proximodistal axis (distal $\bar{x}$ = 192.49 ± 162.87 cm^2, proximal $\bar{x}$ = 174.30 ± 163.78 cm^2, $F_{(1,1404)}$ = 2.606, p = .107). There was no effect of trial on place field frequency ($F_{(4,1195)}$ = 0.289, p = .885) or size ($F_{(4,1404)}$ = 1.085, p = .362) and no trial × region interaction for field frequency ($F_{(4,1195)}$ = 0.390, p = .816) or size

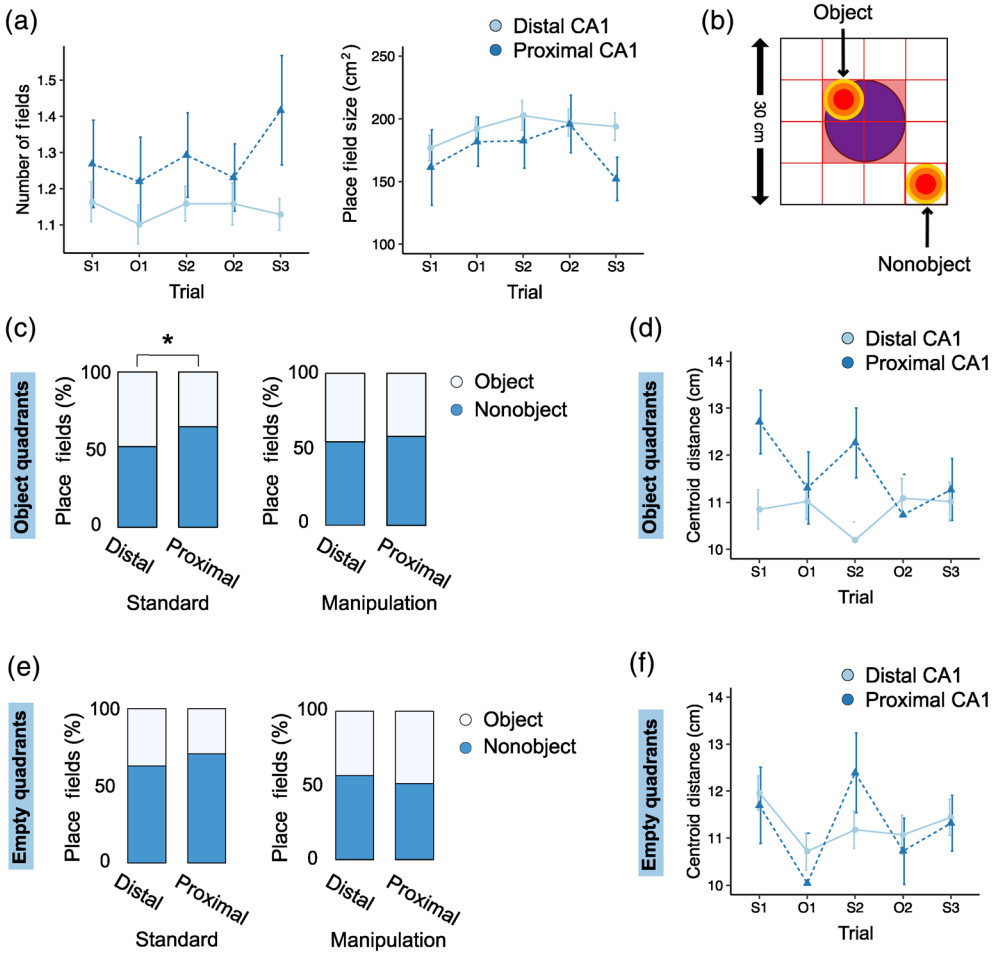

FIGURE 2 Place field frequency and location across the proximodistal axis of CA1. (a) Line plots comparing place field frequency (left) and size (right) across place fields expressed by place cells in distal (light blue, solid line) and proximal CA1 (dark blue, dashed line). Markers (distal = circle, proximal = triangle) represent mean values for each trial. Error bars are SEM. (b) Schematic showing a quadrant of the environment that contains an object with representative place fields from cells that would be categorized as "object" and "nonobject." The grid indicates the division of the quadrant into 16 bins, each of which are 7.5 × 7.5 cm. The central four bins correspond to the object position. (c) Stacked bar plots comparing the proportion of place fields that are expressed in bins of the environment that correspond to the object (light grey) or at other locations in the quadrant (blue) in standard (left) and manipulation trials (right). Data are from fields expressed in quadrants of the environment that contain an object. Asterisk indicates *p*-value <.05 (*). (d) Line plots comparing the distance of place field centroids from the center of the object. (e) Stacked bar plots comparing the proportion of place fields in empty quadrants that are expressed in the four central bins of the environment or at other locations in the quadrant in standard (left) and manipulation trials (right). (f) Line plots comparing the distance of place field centroids from the center of the empty quadrant [Color figure can be viewed at wileyonlinelibrary.com]

($F_{(4,1404)}$ = 0.352, p = .843). The expression of fewer place fields in distal CA1 compared to proximal CA1 is consistent with our observation of higher spatial tuning in this region. Our data suggest that distal CA1 produces more finely tuned spatial maps of environments that contain objects.

Given our observation of higher spatial tuning in distal CA1, we next compared spatial representations of object locations across distal and proximal CA1. The positions of place field centroids were analyzed in relation to object locations for all place fields expressed within quadrants of the environment that contained an object (687 fields [*n* distal = 542, *n* proximal = 145]). For these analyses, each quadrant was divided into 16 bins, where the four central bins corresponded to the object location (Figure 2b). Firstly, we quantified the proportion of place fields with centroids in the central bins of the quadrant ("object" fields) relative to place fields in the bins around the object ("nonobject" fields). The proportion of object fields within object quadrants was greater in distal CA1 than proximal CA1 in standard trials (Figure 2c; distal: 156/324 fields, 48.2%, proximal: 31/87 fields, 35.6%, χ^2 (1) = 4.333, p = .037), but not manipulation trials (distal: 99/218 fields, 45.41%, proximal: 24/58 fields, 41.38%, χ^2 (1) = 0.302, p = .583). However, there were no differences in the proportion of object fields across standard and manipulation trials when compared for distal CA1 (χ^2 (1) = 0.391, p = .532) or proximal CA1 (χ^2 (1) = 0.488, p = .485).

Secondly, we quantified the distance of place field centroids from the object within quadrants that contained objects. Distal CA1 place

fields were nearer to the objects than proximal CA1 place fields (Figure 2d; distal $\bar{x}$ = 10.82 ± 4.19 cm, proximal $\bar{x}$ = 11.69 ± 4.01 cm, $F_{(1,677)}$ = 5.026, p = .025), with no significant effect of trial ($F_{(4,677)}$ = 0.478 p = .7522), or interaction between region and trial ($F_{(4,677)}$ = 1.507, p = .1983). These findings show that distal CA1 place cells express a higher proportion of place fields at object locations than proximal CA1 when object locations are stable, and also that they are closer to objects than proximal CA1 place fields.

One potential explanation for these data is that place fields across the proximodistal axis of CA1 are differentially modulated by boundaries and the difference in distance of place fields from objects is driven by a difference in distance from boundaries. We therefore examined whether place fields were more likely to be expressed in the central bins of object quadrants compared to empty quadrants for each region of CA1. A significantly higher proportion of place field centroids corresponded to the central bins of the object quadrant in distal CA1 (object: 255/542 fields, 47.1%, empty: 245/616 fields, 39.8%, χ^2 (1) = 6.220, p = .013), but not proximal CA1 (object: 55/145 fields, 37.9%, empty: 41/112 fields, 36.6%, χ^2 (1) = 0.047, p = .930). This finding is consistent with our observation of increased firing at object locations in distal CA1.

To control for a potential effect of the boundary of the environment on place field expression, we repeated our analyses for fields expressed within the empty quadrants of the environment (Figure 2e,f). Similar proportions of distal and proximal CA1 place field centroids corresponded to the central bins in standard trials (distal: 140/375 fields, 37.3%, proximal: 21/71 fields, 29.6%, χ^2 (1) = 1.557, p = .212) and manipulation trials (distal: 105/241 fields, 43.6%, proximal: 20/41 fields, 48.8%, χ^2 (1) = 0.386, p = .535). However, there was a significantly higher proportion of fields expressed in the central bins in manipulation trials compared to standard trials for distal CA1 (χ^2 (1) = 21.638, p < .001) and proximal CA1 (χ^2 (1) = 4.130, p = .042). This finding may reflect the firing of place cells in CA1 that encode objects that change location. However, quantification of place field expression across the two types of manipulations revealed no difference in the proportions of fields in the central bins in distal CA1 (O1: 51/117, 43.6%, O2: 54/124 fields, 43.6%, χ^2 (1) = 0.015, p = .902) or proximal CA1 (O1: 8/19 fields, 42.1%, O2: 12/22 fields, 54.6%, χ^2 (1) = 0.632, p = .427). In addition, distal and proximal CA1 place fields were expressed at similar distances from the center of empty quadrants (distal $\bar{x}$ = 11.28 ± 4.35 cm, proximal $\bar{x}$ = 11.30 ± 3.82 cm, $F_{(1,717)}$ = 0.003, p = .959), with no effect of trial ($F_{(4,717)}$ = 1.841, p = .119) and no interaction of region and trial ($F_{(4,717)}$ = 0.592, p = .669). These findings show that our observation that distal CA1 place fields are closer to object locations than proximal CA1 place fields does not persist in empty quadrants and is therefore unlikely to be driven by distance from environment boundaries.

This demonstrates that place fields within quadrants that contain objects are closer to object locations if they receive inputs from LEC rather than MEC. However, one question that remains is whether the two regions have similar proportions of place fields within the object quadrants. Quantification of the proportions of cells within object quadrants revealed that place cells in proximal CA1 expressed a higher proportion of their place fields in the object quadrants in standard trials (distal: 324/699 fields, 46.4%, proximal: 87/158 fields, 55.1%, χ^2 (1) = 3.918, p = .048) and manipulation trials (distal: 218/459 fields, 47.5%, proximal: 58/99 fields, 58.6%, χ^2 (1) = 4.008, p = .045). This may represent an influence of signaling from object-vector cells in MEC (Høydal et al., 2019). Our data demonstrate differences in object representations within entorhinal–hippocampal networks. Proximal CA1 place cells are more likely to fire in quadrants that contain objects, yet distal CA1 place cells that fire within object quadrants express place fields closer to the objects.

We next asked whether differential input from EC modulates place field stability in CA1. We first examined stability across the recording session by comparing correlations between firing rate maps from the first standard trial and all subsequent trials. Our observation of increased spatial tuning in distal CA1 was matched by higher stability of place cells in distal CA1 across trials (Figure 3a,b). The correlations between the first standard trial and subsequent trails were higher in distal CA1 than in proximal CA1 (distal $\bar{x}$ R = 0.576 ± 0.32, proximal $\bar{x}$ R = 0.510 ± 0.31, $F_{(1,951)}$ = 6.041, p = .014). This increased stability was consistent across comparisons with no significant effect of trial ($F_{(3,951)}$ = 1.129, p = .3363) and no significant trial × region interaction ($F_{(3,951)}$ = 0.302, p = .8243). These observations indicate that place cells in distal CA1 maintain more stable spatial representations of environments that contain objects than proximal CA1 place cells.

We next asked if place cell stability is modulated by the proximity of objects. When we examined stability across trials for place cells that have a place field in a quadrant of the environment that contains an object in the first standard trial, there was no main effect of region ($F_{(1,451)}$ = 2.164, p = .142) or trial ($F_{(1,451)}$ = 0.461 p = .710). However, place cells in the hippocampus have been shown to remap when objects are moved in an environment by changing the expression of their place fields (Deshmukh & Knierim, 2013; Lenck-Santini et al., 2005; Manns & Eichenbaum, 2009; Muller & Kubie, 1987). We therefore asked whether remapping responses to local object displacement, rather than objects in general, are different between regions of CA1 receiving different inputs from EC. The proportion of place cells that remapped in the object displacement trial was similar in distal and proximal CA1 (distal: 70/208 cells, 33.7%, proximal: 15/41 cells, 36.6%, (χ^2 (1) = 0.718, p = .856), and the patterns of remapping conformed to those reported previously (Deshmukh & Knierim, 2013; Lenck-Santini et al., 2005; Muller & Kubie, 1987) (Figure 3c). Previous studies have shown that a place cell is more likely to remap when an object is displaced if it expresses a place field near the object before it is moved (Lenck-Santini et al., 2005). Our observation that distal CA1 place fields within object quadrants are closer to objects suggests that remapping in this region could be driven by proximity of place fields to objects in the first standard trial. To examine this possibility, we categorized place cells that expressed place fields in the first standard trial as "near" the object if a place field centroid was located in the quadrant containing the object which would undergo the manipulation (n distal = 46 cells, n proximal = 13 cells), or "far" from the object if all place field centroids were located in the

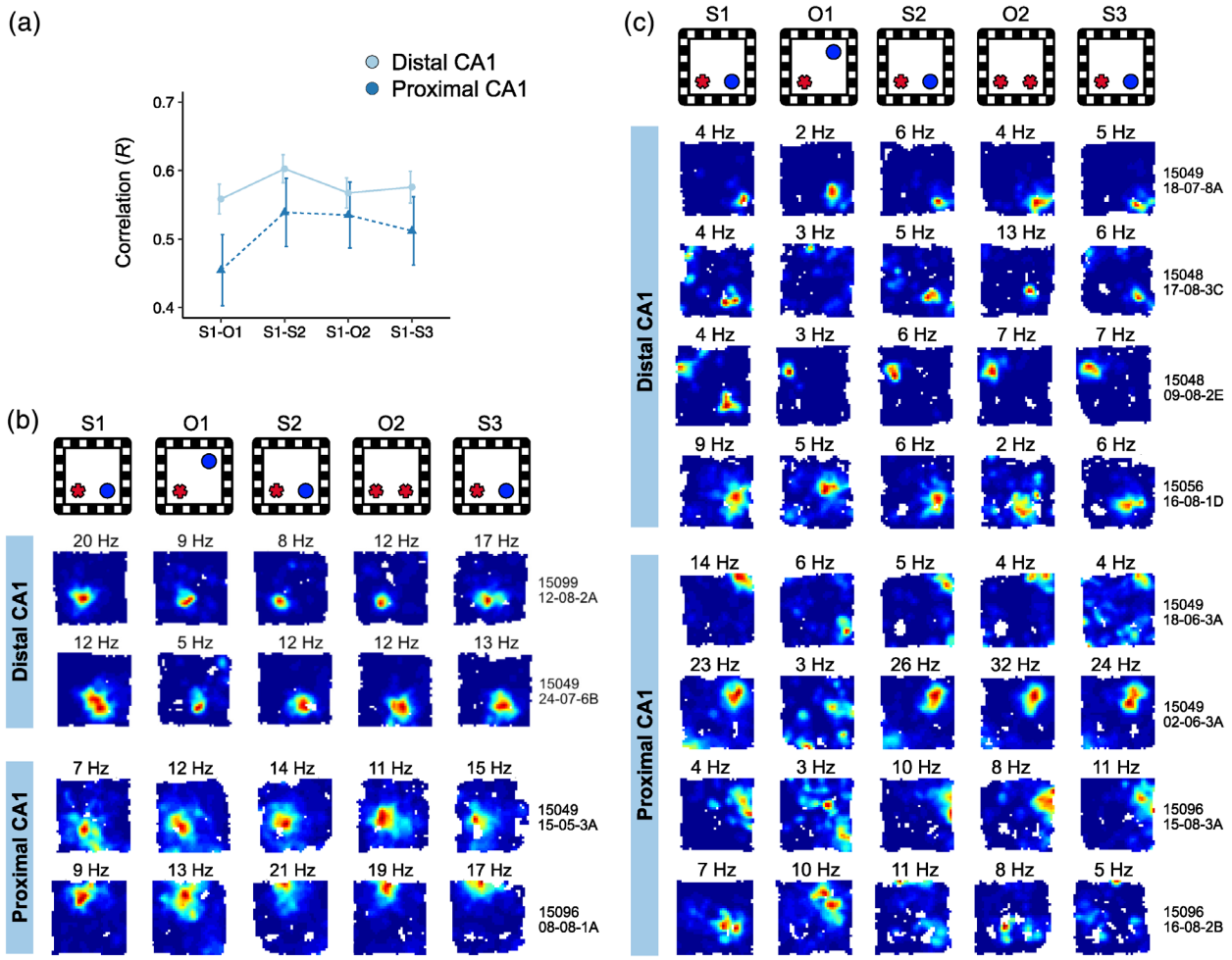

FIGURE 3 Remapping across the proximodistal axis of CA1. (a) Line plots comparing the stability of place cells across the first and second standard trial (S1-S2), first standard trial and object displacement (S1-O1), first standard trial and object-place (S1-O2), and the first and last standard trial for distal (light blue, solid line) and proximal CA1 (dark blue, dashed line). Stability is quantified as the correlation between firing rate maps across trials for each cell, as calculated using Pearson's product–moment coefficient (*R*). Markers (distal = circle, proximal = triangle) represent mean values for each trial. Error bars are SEM. (b) Examples of cells that do not remap in distal (top) and proximal CA1 (bottom). Representative examples are shown that have a correlation value within one standard deviation of the population mean for that region across S1 and O1. Warm colors indicate high firing rates, and cool colors indicate low firing rates or no firing. Peak firing rates for each trial are indicated above the rate maps. (c) Examples of remapping place cells in distal (top) and proximal CA1 (bottom). Representative examples are shown that have a correlation value within one standard deviation of the population mean for remapping cells in that region across S1 and O1 [Color figure can be viewed at wileyonlinelibrary.com]

other quadrants (*n* distal = 133 cells, *n* proximal = 24 cells). Place cells that did not express a field in the first standard trial were excluded from these analyses (*n* distal = 29 cells, *n* proximal = 4 cells). The proportion of cells that remapped in response to object displacement was higher in "near" place cells in distal CA1 (Figure 4a; "near": 21/46 cells, 45.7%, "far": 37/133 cells, 27.8%, χ^2 (1) = 4.962, p = .026), but not proximal CA1 ("near": 5/13 cells, 41.7%, "far": 8/24 cells, 33.33%, χ^2 (1) = 0.097, p = .755). Consistent with this finding, the correlations between rate maps across the first standard trial and object displacement were significantly lower for "near" place cells in distal CA1 (Figure 4b; near $\bar{x}$ R = 0.481 ± 0.339, far $\bar{x}$ R = 0.636 ± 0.282, $F_{(1,177)}$ = 9.215 p = .003), but not proximal CA1 (near $\bar{x}$ R = 0.477 ± 0.319, far $\bar{x}$ R = 0.475 ± 0.353, $F_{(1,35)}$ = 0.0002, p = .989). Finally, we asked how fine-scale the remapping responses to object displacement were in distal CA1 (Figure S3). We examined place field expression across object and nonobject locations, dividing the quadrant into 16 bins, as we described previously (cf. Figure 2b). Within the quadrant that contained the manipulated object, we compared the stability of place cells that expressed place fields at the object location (the four central bins) to those that expressed place fields elsewhere in the quadrant (the outer 12 bins). For comparison, we repeated this analysis within the stable object quadrant and empty quadrants. Place fields were equally stable across central and outer bins in all quadrants. These data suggest that decreased stability in "near" distal CA1 place cells was not specific to those that expressed a place field at the location of the manipulated object. Overall, these data demonstrate

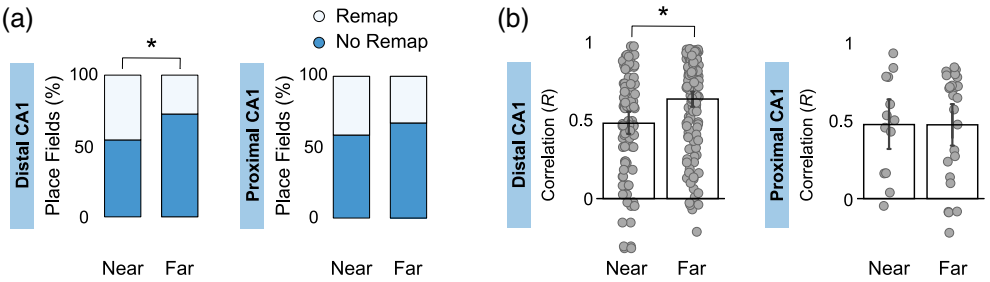

FIGURE 4 Remapping in near and far fields across the proximodistal axis of CA1. (a) Stacked bar plots showing the proportion of remapping cells in distal (left) and proximal CA1 (proximal) that expressed place fields in the first standard trial. Cells were categorized as "near" if they expressed a place field in the object quadrant before it was displaced, and "far" if they only expressed place fields elsewhere in the environment. (b) Bar graphs that compare the average correlation between rate maps across the first standard trial and object displacement for "near" and "far" fields in distal (left) and proximal CA1 (right). Grey dots indicate single place cells. Error bars are SEM. Asterisk indicates *p*-value <.05 (*) [Color figure can be viewed at wileyonlinelibrary.com]

that place cells in both distal and proximal CA1 encode changes in object position. However, the remapping responses to object displacement are modulated by the proximity of place fields to the object in cells that receive inputs from LEC.

Previous studies report that changes in object identity are reflected by changes in firing rate rather than the remapping of place fields (Komorowski & Manns, 2009; Larkin et al., 2014; Manns & Eichenbaum, 2009). LEC neurons encode conjunctive information about object positions in their firing rate (Keene et al., 2016) and LEC lesions alter rate remapping to changes in context in the hippocampus (Lu et al., 2013). These observations raise the possibility that rate coding of novel object-place configurations is stronger in distal CA1. However, for average and peak firing rates there was no main effect of region (average: $F_{(1,1197)}$ = 2.633 p = .105, peak: $F_{(1,1197)}$ = 0.211, p = .646), trial (average: $F_{(4,1197)}$ = 0.750, p = .558, peak: $F_{(4,1197)}$ = 0.730, p = .571) or region × trial interactions (average: $F_{(4,1197)}$ = 0.172, p = .953, peak: $F_{(4,1197)}$ = 0.731, p = .571) (Figure S4). In addition, there were no significant differences between changes in firing rate in distal and proximal CA1 across the first and second standard trials (distal $\bar{x}$ Δ: 0.283 ± 0.228, proximal $\bar{x}$ Δ: 0.258 ± 0.216, $F_{(1,247)}$ = 0.415, p = .520), the first standard trial and object-place recognition (distal $\bar{x}$ Δ: 0.306 ± 0.227, proximal $\bar{x}$ Δ: 0.312 ± 0.199, $F_{(1,234)}$ = 0.022, p = .881), or the second standard trial and object-place recognition (distal $\bar{x}$ Δ: 0.179 ± 0.151, proximal $\bar{x}$ Δ: 0.199 ± 0.150, $F_{(1,234)}$ = 0.588, p = .444) (Figure S3). These data demonstrate that place cells do not show robust rate remapping to changes in object identity in CA1.

A striking feature of hippocampal spatial representations is that a subset of place cells fire at empty locations where an object was previously located (Figure 5a; Deshmukh & Knierim, 2013; O'Keefe, 1976). These cells bear similarity to LEC "trace" cells (Tsao et al., 2013, 2018) and might represent a neural mechanism for object-place memory. We examined trace firing across the proximodistal axis of CA1 to determine whether the characteristics of trace cells differ depending on inputs from EC. Trace cells were observed in similar proportions across distal and proximal CA1 (Figure 5b,c; distal: 38/208 cells, 18.3%, proximal: 10/41 cells, 24.4%, χ^2 (1) = 0.825, p = .364). A subset of trace cells expressed place fields in the newly empty quadrant in the object displacement trial, consistent with the "misplace" cells described by O'Keefe (1976). Misplace cells were observed at similar frequencies across distal and proximal CA1 (distal: 15/38 trace cells, 39.5%, proximal: 5/10 trace cells, 50.0%, χ^2 (1) =0.361, p = .548). A second subset of trace cells expressed a place field in the novel quadrant, consistent with the "object-place memory" cells described by Deshmukh and Knierim (2013). Object-place memory cells were observed at similar frequencies across distal and proximal CA1 (distal: 25/38 cells, 65.8%, proximal: 5/10 cells, 50.0%, χ^2 (1) = 0.842, p = .359), and could be further divided into two groups. Some object-place memory cells immediately remapped to express a place field in the novel quadrant when the object was moved, and persisted firing in that quadrant in subsequent trials after the object was returned to its original location ("remap trace" cells). However, some cells expressed a new place field in the empty novel quadrant, but only after the object was returned to its original location ("nonremap trace" cells). Although most trace cells could be categorized as misplace or object-place memory cells, a subset of distal CA1 place cells manifested both types of trace behavior (2/38 cells, 5.3%).

Given our observation that distal CA1 place cells are more selective for object locations and that remapping in this region is modulated by the proximity of place fields to objects, we hypothesized that trace cells in distal CA1 may more precisely encode previous object location than trace cells in proximal CA1. To explore this possibility, we measured the distances of place fields expressed in the empty quadrant from the previous object location. For misplace cells, place fields were expressed at similar distances from the previous object location in distal and proximal CA1 (Figure 5d; distal $\bar{x}$ = 11.61 ± 4.68 cm, proximal $\bar{x}$ = 11.48 ± 3.81 cm, $F_{(1,19)}$ = 0.004, p = .950). However, the place fields expressed by object-place memory cells in distal CA1 were significantly closer to the empty object location than those expressed in proximal CA1 (distal $\bar{x}$ = 10.32 ± 4.39 cm, proximal $\bar{x}$ = 13.46 ± 2.01 cm, $F_{(1,66)}$ = 5.368, p = .024). Consistent with these findings, the centroid locations of place fields in distal CA1 were more likely to correspond to the

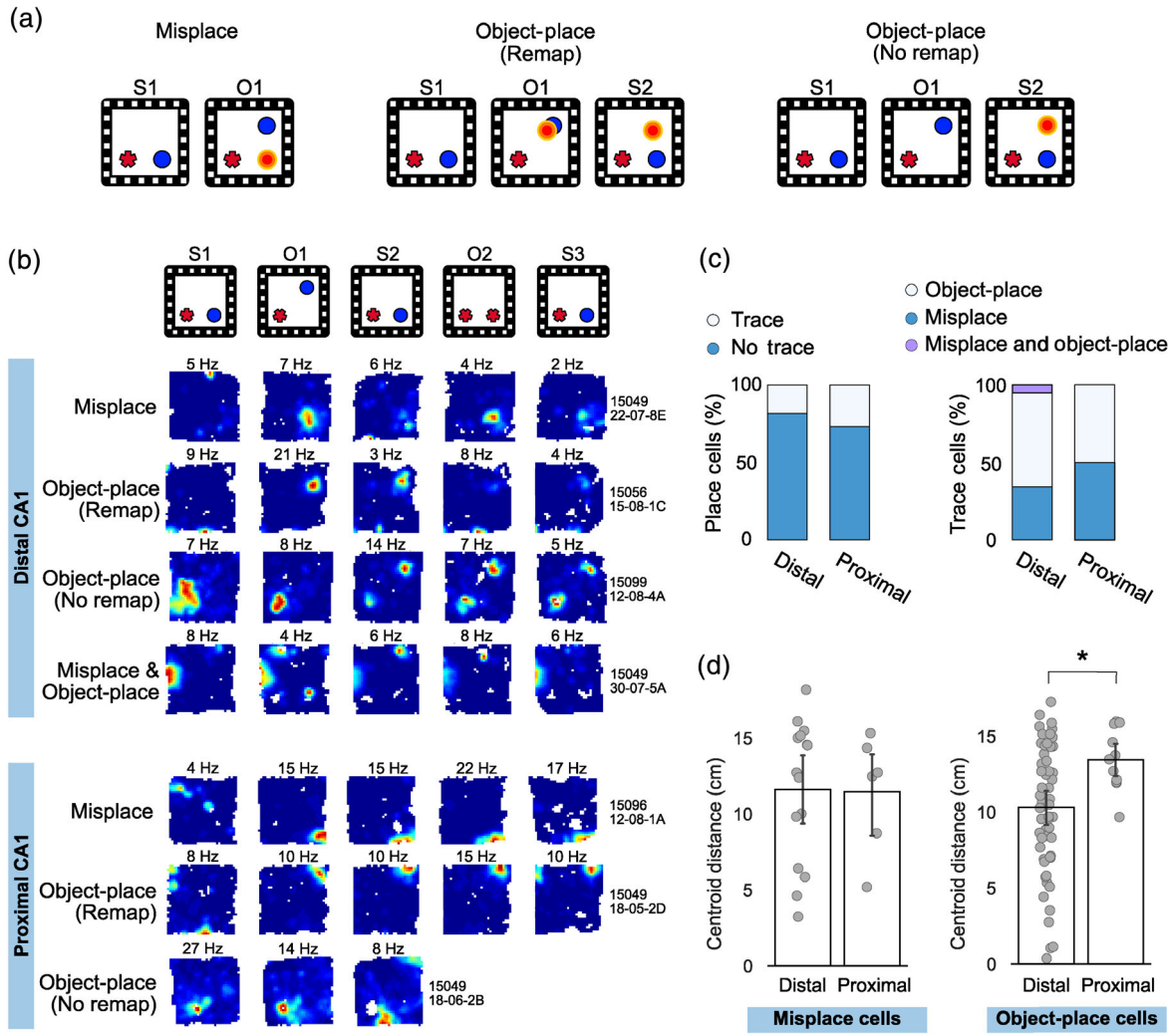

FIGURE 5 Trace firing across the proximodistal axis of CA1. (a) Schematic showing cartoon example of misplace firing (left) and object-place memory firing with remapping in the object displacement trial (middle) and without remapping (right). (b) Examples of trace firing in distal (top) and proximal CA1 (bottom). Examples of misplace and object-place memory cells (with and without remapping) are included for each region. Warm colors indicate high firing rates, and cool colors indicate low firing rates or no firing. Peak firing rates for each trial are indicated above the rate maps. (c) Stacked bar charts indicate the proportion of place cells in each region of CA1 with trace firing (left) and the relative proportions of these which conformed to patterns consistent with misplace firing and trace firing at the empty novel object location (right). (d) Bar plots show the average distance of place field centroids from the empty object location for misplace (left) and object-place memory cells which fire at the empty novel object location (right). Each grey dot represents a single place field. Asterisk indicates a *p*-value <.05 (*) [Color figure can be viewed at wileyonlinelibrary.com]

previous object location for object-place memory cells (distal: 29/57 fields, 50.9%, proximal: 2/14 fields, 14.3%, χ^2 (1) = 6.1179, p = .013), but not misplace cells (distal: 6/15 fields, 40.0%, proximal: 2/6 fields, 33.3%, χ^2 (1) = 0.081, p = .776). These data demonstrate that CA1 place cells receiving input from LEC generate representations of previous object locations that are closer to the previous object location than those that receive input from MEC.

4 | DISCUSSION

Our data provide evidence that the spatial representations of cue-rich environments generated by place cells in CA1 show different characteristics in regions that receive inputs from different parts of EC. Place cells in distal CA1, which receive inputs from LEC, generated representations of object locations that were closer to the objects than place cells in proximal CA1 that are downstream from MEC. Place cells in distal CA1 demonstrated higher spatial tuning and were more stable across trials then proximal CA1 place cells. In addition, place cell stability in distal CA1 was modulated by the proximity of place fields to objects; place cells that fired in the quadrant containing the manipulated object were significantly less stable than place cells with fields elsewhere in the environment. Distance-based modulation of place cell stability was not observed in proximal CA1. Trace cells were recorded in both regions of CA1, but trace fields were closer to the previous location of objects in distal CA1. Overall, our findings

suggest that the presence of objects in the local environment results in higher spatial tuning and greater proximity of distal CA1 place cell representations to both current object locations and the locations where objects were previously encountered. These findings are interesting in light of previous findings of increased spatial tuning in proximal CA1 in empty environments (Henriksen et al., 2010). Future studies could directly address how spatial representations of empty environments are changed by the introduction of objects.

Before addressing the implication of the current findings for our understanding of hippocampal–entorhinal interactions it should be noted that the current experiment does not control for changes in behavior caused by changing mnemonic status of the objects within trials. At the beginning of manipulation trials animals encounter objects that are either in a novel or familiar spatial configuration and this results in a bias towards exploration of the novel configuration. As the trial progresses the relative familiarity of these configurations changes and this change in mnemonic status changes patterns of object exploration. It is possible that differences in behavior induced by these mnemonic changes could affect spatial representations in CA1. In the current study, however, the critical comparison is between place cell representations in proximal and distal CA1. These representations will be equally affected by the behavioral changes induced by changes in mnemonic status of the objects, therefore this does not detract from the findings of the study.

These results inform our understanding of information processing within the EC-hippocampal network. Our data suggest that models describing the combination of spatial information from MEC with non-spatial information from LEC within the hippocampus are overly simplistic (Ainge et al., 2012; Ainge, Tamosiunaite, et al., 2007; Ainge, van der Meer, et al., 2007; Eichenbaum et al., 2012; Ferbinteanu & Shapiro, 2003; Hargreaves et al., 2005; Hasselmo, 2009; Hayman & Jeffery, 2008; Kerr et al., 2007; Knierim et al., 2006; Leutgeb et al., 2005). Our findings show that the binding of item information into spatial context is not uniform across the hippocampus. These data are consistent with reports of differential functional properties across the proximodistal axis of CA1 (Beer et al., 2018; Hartzell et al., 2013; Henriksen et al., 2010; Ito & Schuman, 2012; Nakamura et al., 2013; Nakazawa et al., 2016) and suggest that the precise integration of item and spatial information necessary for episodic memory may be a specialized function of specific networks within the hippocampus.

Our data also have implications for the use of object information within the EC-hippocampal network. Information about objects is suggested to originate in perirhinal cortex (PRh) (Brown & Aggleton, 2001; Brown et al., 2010), a structure that is required for novel object recognition (Ennaceur et al., 1996; Mumby & Glenn, 2000; Norman & Eacott, 2005; Wan et al., 1999; Winters et al., 2004) and contains single neurons that respond to objects (Ahn & Lee, 2015; Bogacz et al., 2001; Bogacz & Brown, 2003; Burke et al., 2012; Deshmukh et al., 2012). PRh provides major input into LEC but also significant input into MEC and some direct input into hippocampus (Burwell & Amaral, 1998a, 1998b; Furtak et al., 2007; Kosel et al., 1983). It is therefore unlikely that object information reaches the hippocampus from PRh exclusively through connectivity with LEC. Consistent with this, both LEC and MEC encode information about objects in the environment yet manifest distinct patterns of object-modulated firing. LEC neurons generate representations of current object positions and encode locations in the environment where objects were previously experienced (Deshmukh & Knierim, 2013; Tsao et al., 2013, 2018). In contrast, spatial frameworks generated in MEC are tied to environmental stimuli (Chen et al., 2016; Hafting et al., 2005; Pérez-Escobar et al., 2016) and single cells encode vector relationships between objects and an animal's position (Høydal et al., 2019). Signaling from object-responsive cells in MEC and LEC might drive different patterns of object modulation across the proximodistal axis of CA1. Our data suggest a model where object information from LEC supports the generation of spatial representations in distal CA1 that have higher levels of spatial tuning and closer proximity to object locations. In parallel, object vector signaling from MEC generates place cell representations in proximal CA1 that are less spatially tuned in the presence of objects and less stable across trials.

This suggestion is consistent with previous studies proposing that LEC and MEC support local and global spatial frameworks, respectively (Knierim et al., 2014; Knierim & Hamilton, 2011; Neunuebel et al., 2013). Neunuebel et al. (2013) showed that when local and global cues were put into conflict, the activity of LEC neurons was weakly modulated by local cues, whereas the activity of MEC neurons was modulated by global cues. Consistent with this, Kuruvilla and Ainge (2017) showed that lesions of LEC, but not MEC, impaired rat's ability to use local spatial frameworks to guide behavior. However, anatomical studies suggest a different interpretation of these findings. LEC receives extensive inputs from olfactory areas, whereas MEC receives inputs that carry predominantly visual information (Canto et al., 2008; Kerr et al., 2007; van Strien et al., 2009). This suggests that representations of environmental stimuli within LEC and MEC are based on different combinations of sensory modalities. In our experiments, objects served as local cues from which rats could sample both visual and olfactory features. Global cues were large objects within the lab from which rats could only extract visual features. Our findings of more precise spatial tuning in place cells that receive LEC input could be driven by those cells having more sensory information (olfactory and visual) from which to construct spatial representations. This would be consistent with place fields being in closer proximity to objects in distal CA1 as these fields would be driven by sensory information that can only be sampled at close range. Whether the distinction between information processing in LEC and MEC is best described in terms of spatial scale (local vs. global) or sensory modality (olfactory vs. visual) remains to be determined.

Recent studies have conceptualized differences in LEC and MEC information processing in terms of egocentric and allocentric spatial frameworks. Wang et al. (2018) analyzed spatial frameworks of neurons recorded from LEC and MEC and showed that LEC neurons robustly encoded egocentric space while MEC was more responsive

to allocentric cues. Kuruvilla et al. (2020) tested how egocentric and allocentric spatial frameworks support object-location memory in rats. Rats were presented with an object-location memory test from a familiar or novel perspective. Presenting the test environment from a novel perspective forces the rat to orient itself in allocentric space before performing the task, whereas presentation from a familiar perspective encourages the use of an egocentric strategy. Rats with LEC lesions were impaired on the egocentric version, but performed above chance in the allocentric version. Given that egocentric space is governed largely by local cues, this is consistent with our finding that an LEC-distal CA1 network precisely encodes the location of objects within the immediate environment whereas MEC-proximal CA1 networks encode objects in reference to allocentric spatial frameworks.

Our observations raise further questions regarding how object-related responses in CA1 relate to the memory and navigation functions performed within the EC-hippocampal network. LEC is required to integrate different features of an episode (Chao et al., 2016; Kuruvilla & Ainge, 2017; Rodo et al., 2017; Van Cauter et al., 2013; Vandrey et al., 2020; Wilson, Langston, et al., 2013; Wilson, Watanabe, et al., 2013), and our data further suggest that the multimodal representations generated in LEC support place field representations in distal CA1 that precisely encode items within an environment. Furthermore, the precise representations of previous object locations in distal CA1 suggest a role of LEC-hippocampus circuitry in object-place memory. Our findings are consistent with a role of projections from LEC to the hippocampus in episodic memory (Vandrey et al., 2020) and with reports that LEC manifests early pathology in Alzheimer's disease (Gómez-Isla et al., 1996; Khan et al., 2014; Kobro-Flatmoen et al., 2016; Stranahan & Mattson, 2010). In contrast, MEC is part of a network that supports path integration, navigation, and spatial memory (Hales et al., 2014; Steffenach et al., 2005; Tennant et al., 2018; Van Cauter et al., 2013). Our data suggest that spatial representations generated in MEC drive spatial representations in proximal CA1 that are less tuned to local features. This is consistent with the utility of nonlocal cues for navigation and spatial memory, where global cues provide consistent spatial information when navigating over longer distances.

ACKNOWLEDGMENTS

This work was supported by a Henry Dryerre scholarship from the Royal Society of Edinburgh to B. Vandrey.

CONFLICT OF INTEREST

The authors declared no potential conflicts of interest.

AUTHOR CONTRIBUTIONS

Conceptualization and methodology: B.V., J.A.; investigation: B.V.; writing - original draft: B.V., J.A.; analysis: B.V., S.D.; writing, review, and editing: B.V., S.D., J.A.; supervision: J.A.; funding acquisition: B.V.

DATA AVAILABILITY STATEMENT

The data that support the findings of this study are available from the corresponding author upon reasonable request.

ORCID

James A. Ainge https://orcid.org/0000-0002-0007-1533

REFERENCES

Ahn, J.-R., & Lee, I. (2015). Neural correlates of object-associated choice behavior in the perirhinal cortex of rats. *The Journal of Neuroscience*, *35*(4), 1692–1705. https://doi.org/10.1523/JNEUROSCI.3160-14.2015

Ainge, J. A., Tamosiunaite, M., Woergoetter, F., & Dudchenko, P. A. (2007). Hippocampal CA1 place cells encode intended destination on a maze with multiple choice points. *The Journal of Neuroscience*, *27*(36), 9769–9779. https://doi.org/10.1523/JNEUROSCI.2011-07.2007

Ainge, J. A., Tamosiunaite, M., Wörgötter, F., & Dudchenko, P. A. (2012). Hippocampal place cells encode intended destination, and not a discriminative stimulus, in a conditional T-maze task. *Hippocampus*, *22*(3), 534–543. https://doi.org/10.1002/hipo.20919

Ainge, J. A., van der Meer, M. A. A., Langston, R. F., & Wood, E. R. (2007). Exploring the role of context-dependent hippocampal activity in spatial alternation behavior. *Hippocampus*, *17*(10), 988–1002. https://doi.org/10.1002/hipo.20301

Aggleton, J. P., & Nelson, A. J. D. (2020). Distributed interactive brain circuits for object-in-place memory: A place for time? *Brain and Neuroscience Advances*, *4*, 1–11. https://doi.org/10.1177/2398212820933471

Barker, G. R. I., Banks, P. J., Scott, H., Ralph, G. S., Mitrophanous, K. A., Wong, L.-F., Bashir, Z. I., Uney, J. B., & Warburton, E. C. (2017). Separate elements of episodic memory subserved by distinct hippocampal-prefrontal connections. *Nature Neuroscience*, *20*(2), 242–250. https://doi.org/10.1038/nn.4472

Barker, G. R. I., & Warburton, E. C. (2011). When is the hippocampus involved in recognition memory? *The Journal of Neuroscience*, *31*(29), 10721–10731. https://doi.org/10.1523/JNEUROSCI.6413-10.2011

Beer, Z., Vavra, P., Atucha, E., Rentzing, K., Heinze, H.-J., & Sauvage, M. M. (2018). The memory for time and space differentially engages the proximal and distal parts of the hippocampal subfields CA1 and CA3. *PLoS Biology*, *16*(8), e2006100. https://doi.org/10.1371/journal.pbio.2006100

Bogacz, R., & Brown, M. W. (2003). Comparison of computational models of familiarity discrimination in the perirhinal cortex. *Hippocampus*, *13*(4), 494–524. https://doi.org/10.1002/hipo.10093

Bogacz, R., Brown, M. W., & Giraud-Carrier, C. (2001). Model of familiarity discrimination in the perirhinal cortex. *Journal of Computational Neuroscience*, *10*(1), 5–23. https://doi.org/10.1023/a:1008925909305

Brown, M. W., & Aggleton, J. P. (2001). Recognition memory: What are the roles of the perirhinal cortex and hippocampus? *Nature Reviews. Neuroscience*, *2*(1), 51–61.

Brown, M. W., Warburton, E. C., & Aggleton, J. P. (2010). Recognition memory: Material, processes, and substrates. *Hippocampus*, *20*(11), 1228–1244. https://doi.org/10.1002/hipo.20858

Burke, S. N., Maurer, A. P., Hartzell, A. L., Nematollahi, S., Uprety, A., Wallace, J. L., & Barnes, C. A. (2012). Representation of three-dimensional objects by the rat perirhinal cortex. *Hippocampus*, *22*(10), 2032–2044. https://doi.org/10.1002/hipo.22060

Burke, S. N., Maurer, A. P., Nematollahi, S., Uprety, A. R., Wallace, J. L., & Barnes, C. A. (2011). The influence of objects on place field expression and size in distal hippocampal CA1. *Hippocampus*, *21*(7), 783–801. https://doi.org/10.1002/hipo.20929

Burwell, R. D., & Amaral, D. G. (1998a). Cortical afferents of the perirhinal, postrhinal, and entorhinal cortices of the rat. *The Journal of Comparative Neurology*, *398*(2), 179–205.

Burwell, R. D., & Amaral, D. G. (1998b). Perirhinal and postrhinal cortices of the rat: Interconnectivity and connections with the entorhinal cortex. *The Journal of Comparative Neurology*, *391*(3), 293–321. https://doi.org/10.1002/(sici)1096-9861(19980216)391:3<293::aid-cne2>3.0.co;2-x

Canto, C. B., Wouterlood, F. G., & Witter, M. P. (2008). What does the anatomical organization of the entorhinal cortex tell us? *Neural Plasticity*, *2008*, 381243. https://doi.org/10.1155/2008/381243

Chao, O. Y., Huston, J. P., Li, J.-S., Wang, A.-L., & de Souza Silva, M. A. (2016). The medial prefrontal cortex-lateral entorhinal cortex circuit is essential for episodic-like memory and associative object-recognition. *Hippocampus*, *26*(5), 633–645. https://doi.org/10.1002/hipo.22547

Chen, G., Manson, D., Cacucci, F., & Wills, T. J. (2016). Absence of visual input results in the disruption of grid cell firing in the mouse. *Current Biology: CB*, *26*(17), 2335–2342. https://doi.org/10.1016/j.cub.2016.06.043

Deshmukh, S. S., Johnson, J. L., & Knierim, J. J. (2012). Perirhinal cortex represents nonspatial, but not spatial, information in rats foraging in the presence of objects: Comparison with lateral entorhinal cortex. *Hippocampus*, *22*(10), 2045–2058. https://doi.org/10.1002/hipo.22046

Deshmukh, S. S., & Knierim, J. J. (2011). Representation of non-spatial and spatial information in the lateral entorhinal cortex. *Frontiers in Behavioral Neuroscience*, *5*, 69. https://doi.org/10.3389/fnbeh.2011.00069

Deshmukh, S. S., & Knierim, J. J. (2013). Influence of local objects on hippocampal representations: Landmark vectors and memory. *Hippocampus*, *23*(4), 253–267. https://doi.org/10.1002/hipo.22101

Eacott, M. J., & Norman, G. (2004). Integrated memory for object, place, and context in rats: A possible model of episodic-like memory? *The Journal of Neuroscience*, *24*(8), 1948–1953. https://doi.org/10.1523/JNEUROSCI.2975-03.2004

Eichenbaum, H., Sauvage, M., Fortin, N., Komorowski, R., & Lipton, P. (2012). Towards a functional organization of episodic memory in the medial temporal lobe. *Neuroscience and Biobehavioral Reviews*, *36*(7), 1597–1608. https://doi.org/10.1016/j.neubiorev.2011.07.006

Ennaceur, A., & Delacour, J. (1988). A new one-trial test for neurobiological studies of memory in rats. 1: Behavioral data. *Behavioural Brain Research*, *31*(1), 47–59. https://www.ncbi.nlm.nih.gov/pubmed/3228475

Ennaceur, A., Neave, N., & Aggleton, J. P. (1996). Neurotoxic lesions of the perirhinal cortex do not mimic the behavioural effects of fornix transection in the rat. *Behavioural Brain Research*, *80*(1), 9–25. https://doi.org/10.1016/0166-4328(96)00006-X

Ferbinteanu, J., & Shapiro, M. L. (2003). Prospective and retrospective memory coding in the hippocampus. *Neuron*, *40*(6), 1227–1239. https://doi.org/10.1016/s0896-6273(03)00752-9

Furtak, S. C., Wei, S.-M., Agster, K. L., & Burwell, R. D. (2007). Functional neuroanatomy of the parahippocampal region in the rat: The perirhinal and postrhinal cortices. *Hippocampus*, *17*(9), 709–722. https://doi.org/10.1002/hipo.20314

Gómez-Isla, T., Price, J. L., McKeel, D. W., Jr., Morris, J. C., Growdon, J. H., & Hyman, B. T. (1996). Profound loss of layer II entorhinal cortex neurons occurs in very mild Alzheimer's disease. *The Journal of Neuroscience*, *16*(14), 4491–4500. https://www.ncbi.nlm.nih.gov/pubmed/8699259

Hafting, T., Fyhn, M., Molden, S., Moser, M.-B., & Moser, E. I. (2005). Microstructure of a spatial map in the entorhinal cortex. *Nature*, *436*(7052), 801–806. https://doi.org/10.1038/nature03721

Hales, J. B., Schlesiger, M. I., Leutgeb, J. K., Squire, L. R., Leutgeb, S., & Clark, R. E. (2014). Medial entorhinal cortex lesions only partially disrupt hippocampal place cells and hippocampus-dependent place memory. *Cell Reports*, *9*(3), 893–901. https://doi.org/10.1016/j.celrep.2014.10.009

Hargreaves, E. L., Rao, G., Lee, I., & Knierim, J. J. (2005). Major dissociation between medial and lateral entorhinal input to dorsal hippocampus. *Science*, *308*(5729), 1792–1794. https://science.sciencemag.org/content/308/5729/1792.short

Hartzell, A. L., Burke, S. N., Hoang, L. T., Lister, J. P., Rodriguez, C. N., & Barnes, C. A. (2013). Transcription of the immediate-early gene arc in CA1 of the hippocampus reveals activity differences along the proximodistal axis that are attenuated by advanced age. *The Journal of Neuroscience*, *33*(8), 3424–3433. https://doi.org/10.1523/JNEUROSCI.4727-12.2013

Hasselmo, M. E. (2009). A model of episodic memory: Mental time travel along encoded trajectories using grid cells. *Neurobiology of Learning and Memory*, *92*(4), 559–573. https://doi.org/10.1016/j.nlm.2009.07.005

Hayman, R. M., & Jeffery, K. J. (2008). How heterogeneous place cell responding arises from homogeneous grids—A contextual gating hypothesis. *Hippocampus*, *18*(12), 1301–1313. https://doi.org/10.1002/hipo.20513

Henriksen, E. J., Colgin, L. L., Barnes, C. A., Witter, M. P., Moser, M.-B., & Moser, E. I. (2010). Spatial representation along the proximodistal axis of CA1. *Neuron*, *68*(1), 127–137. https://doi.org/10.1016/j.neuron.2010.08.042

Høydal, Ø. A., Skytøen, E. R., Andersson, S. O., Moser, M.-B., & Moser, E. I. (2019). Object-vector coding in the medial entorhinal cortex. *Nature*, *568*(7752), 400–404. https://doi.org/10.1038/s41586-019-1077-7

Ito, H. T., & Schuman, E. M. (2012). Functional division of hippocampal area CA1 via modulatory gating of entorhinal cortical inputs. *Hippocampus*, *22*(2), 372–387. https://doi.org/10.1002/hipo.20909

Keene, C. S., Bladon, J., McKenzie, S., Liu, C. D., O'Keefe, J., & Eichenbaum, H. (2016). Complementary functional organization of neuronal activity patterns in the perirhinal, lateral entorhinal, and medial entorhinal cortices. *The Journal of Neuroscience*, *36*(13), 3660–3675. https://doi.org/10.1523/JNEUROSCI.4368-15.2016

Kerr, K. M., Agster, K. L., Furtak, S. C., & Burwell, R. D. (2007). Functional neuroanatomy of the parahippocampal region: The lateral and medial entorhinal areas. *Hippocampus*, *17*(9), 697–708. https://doi.org/10.1002/hipo.20315

Khan, U. A., Liu, L., Provenzano, F. A., Berman, D. E., Profaci, C. P., Sloan, R., Mayeux, R., Duff, S. A., & Small, S. A. (2014). Molecular drivers and cortical spread of lateral entorhinal cortex dysfunction in preclinical Alzheimer's disease. *Nature Neuroscience*, *17*(2), 304–311. https://doi.org/10.1038/nn.3606

Knierim, J. J., & Hamilton, D. A. (2011). Framing spatial cognition: Neural representations of proximal and distal frames of reference and their roles in navigation. *Physiological Reviews*, *91*(4), 1245–1279. https://doi.org/10.1152/physrev.00021.2010

Knierim, J. J., Lee, I., & Hargreaves, E. L. (2006). Hippocampal place cells: Parallel input streams, subregional processing, and implications for episodic memory. *Hippocampus*, *16*(9), 755–764. https://onlinelibrary.wiley.com/doi/abs/10.1002/hipo.20203

Knierim, J. J., Neunuebel, J. P., & Deshmukh, S. S. (2014). Functional correlates of the lateral and medial entorhinal cortex: Objects, path integration and local–global reference frames. *Philosophical Transactions of the Royal Society of London. Series B, Biological Sciences*, *369*(1635), 20130369. https://doi.org/10.1098/rstb.2013.0369

Kobro-Flatmoen, A., Nagelhus, A., & Witter, M. P. (2016). Reelin-immunoreactive neurons in entorhinal cortex layer II selectively express intracellular amyloid in early Alzheimer's disease. *Neurobiology of Disease*, *93*, 172–183. https://doi.org/10.1016/j.nbd.2016.05.012

Komorowski, R. W., & Manns, J. R. (2009). Robust conjunctive item–place coding by hippocampal neurons parallels learning what happens where. *Journal of Neuroscience*, *29*(31), 9918–9929.

Kosel, K. C., Van Hoesen, G. W., & Rosene, D. L. (1983). A direct projection from the perirhinal cortex (area 35) to the subiculum in the rat. *Brain Research*, *269*(2), 347–351.

Kuruvilla, M. V., & Ainge, J. A. (2017). Lateral entorhinal cortex lesions impair local spatial frameworks. *Frontiers in Systems Neuroscience*, *11*, 30. https://doi.org/10.3389/fnsys.2017.00030

Kuruvilla, M. V., Wilson, D. I. G., & Ainge, J. A. (2020). Lateral entorhinal cortex lesions impair both egocentric and allocentric object-place

associations. *Brain and Neuroscience Advances*, *4*, 1–11. https://doi.org/10.1177/2398212820939463

Langston, R. F., & Wood, E. R. (2010). Associative recognition and the hippocampus: Differential effects of hippocampal lesions on object-place, object-context and object-place-context memory. *Hippocampus*, *20* (10), 1139–1153. https://doi.org/10.1002/hipo.20714

Larkin, M. C., Lykken, C., Tye, L. D., Wickelgren, J. G., & Frank, L. M. (2014). Hippocampal output area CA1 broadcasts a generalized novelty signal during an object-place recognition task. *Hippocampus*, *24*, 773–783. https://doi.org/10.1002/hipo.22268

Lenck-Santini, P.-P., Rivard, B., Muller, R. U., & Poucet, B. (2005). Study of CA1 place cell activity and exploratory behavior following spatial and nonspatial changes in the environment. *Hippocampus*, *15*(3), 356–369. https://doi.org/10.1002/hipo.20060

Leutgeb, S., Leutgeb, J. K., Barnes, C. A., Moser, E. I., McNaughton, B. L., & Moser, M.-B. (2005). Independent codes for spatial and episodic memory in hippocampal neuronal ensembles. *Science*, *309*(5734), 619–623. https://doi.org/10.1126/science.1114037

Lu, L., Leutgeb, J. K., Tsao, A., Henriksen, E. J., Leutgeb, S., Barnes, C. A., Witter, M. P., Moser, M.-B., & Moser, E. I. (2013). Impaired hippocampal rate coding after lesions of the lateral entorhinal cortex. *Nature Neuroscience*, *16*(8), 1085–1093. https://doi.org/10.1038/nn.3462

Manns, J. R., & Eichenbaum, H. (2006). Evolution of declarative memory. *Hippocampus*, *16*(9), 795–808. https://doi.org/10.1002/hipo.20205

Manns, J. R., & Eichenbaum, H. (2009). A cognitive map for object memory in the hippocampus. *Learning & Memory*, *16*(10), 616–624. https://doi.org/10.1101/lm.1484509

Masurkar, A. V., Srinivas, K. V., Brann, D. H., Warren, R., Lowes, D. C., & Siegelbaum, S. A. (2017). Medial and lateral entorhinal cortex differentially excite deep versus superficial CA1 pyramidal neurons. *Cell Reports*, *18*(1), 148–160. https://doi.org/10.1016/j.celrep.2016.12.012

Michael Wyss, J. (1981). An autoradiographic study of the efferent connections of the entorhinal cortex in the rat. *The Journal of Comparative Neurology*, *199*(4), 495–512. https://doi.org/10.1002/cne.901990405

Muller, R. U., & Kubie, J. L. (1987). The effects of changes in the environment on the spatial firing of hippocampal complex-spike cells. *The Journal of Neuroscience*, *7*(7), 1951–1968. https://www.ncbi.nlm.nih.gov/pubmed/3612226

Mumby, D. G., Gaskin, S., Glenn, M. J., Schramek, T. E., & Lehmann, H. (2002). Hippocampal damage and exploratory preferences in rats: Memory for objects, places, and contexts. *Learning & Memory*, *9*(2), 49–57. https://doi.org/10.1101/lm.41302

Mumby, D. G., & Glenn, M. J. (2000). Anterograde and retrograde memory for object discriminations and places in rats with perirhinal cortex lesions. *Behavioural Brain Research*, *114*, 119–134. https://doi.org/10.1016/s0166-4328(00)00217-5

Naber, P. A., Lopes da Silva, F. H., & Witter, M. P. (2001). Reciprocal connections between the entorhinal cortex and hippocampal fields CA1 and the subiculum are in register with the projections from CA1 to the subiculum. *Hippocampus*, *11*(2), 99–104. https://doi.org/10.1002/hipo.1028

Nakamura, N. H., Flasbeck, V., Maingret, N., Kitsukawa, T., & Sauvage, M. M. (2013). Proximodistal segregation of nonspatial information in CA3: Preferential recruitment of a proximal CA3-distal CA1 network in nonspatial recognition memory. *The Journal of Neuroscience*, *33*(28), 11506–11514. https://doi.org/10.1523/JNEUROSCI.4480-12.2013

Nakazawa, Y., Pevzner, A., Tanaka, K. Z., & Wiltgen, B. J. (2016). Memory retrieval along the proximodistal axis of CA1. *Hippocampus*, *26*(9), 1140–1148. https://doi.org/10.1002/hipo.22596

Neunuebel, J. P., Yoganarasimha, D., Rao, G., & Knierim, J. J. (2013). Conflicts between local and global spatial frameworks dissociate neural representations of the lateral and medial entorhinal cortex. *The Journal of Neuroscience*, *33*(22), 9246–9258. https://doi.org/10.1523/JNEUROSCI.0946-13.2013

Norman, G., & Eacott, M. J. (2005). Dissociable effects of lesions to the perirhinal cortex and the postrhinal cortex on memory for context and objects in rats. *Behavioral Neuroscience*, *119*(2), 557–566. https://doi.org/10.1037/0735-7044.119.2.557

O'Keefe, J. (1976). Place units in the hippocampus of the freely moving rat. *Experimental Neurology*, *51*(1), 78–109. https://www.ncbi.nlm.nih.gov/pubmed/1261644

Pérez-Escobar, J. A., Kornienko, O., Latuske, P., Kohler, L., & Allen, K. (2016). Visual landmarks sharpen grid cell metric and confer context specificity to neurons of the medial entorhinal cortex. *eLife*, *5*, 1–21. https://doi.org/10.7554/eLife.16937

Rodo, C., Sargolini, F., & Save, E. (2017). Processing of spatial and non-spatial information in rats with lesions of the medial and lateral entorhinal cortex: Environmental complexity matters. *Behavioural Brain Research*, *320*, 200–209. https://doi.org/10.1016/j.bbr.2016.12.009

Save, E., Buhot, M. C., Foreman, N., & Thinus-Blanc, C. (1992). Exploratory activity and response to a spatial change in rats with hippocampal or posterior parietal cortical lesions. *Behavioural Brain Research*, *47*(2), 113–127. https://doi.org/10.1016/s0166-4328(05)80118-4

Schmitzer-Torbert, N., Jackson, J., Henze, D., Harris, K., & Redish, A. D. (2005). Quantitative measures of cluster quality for use in extracellular recordings. *Neuroscience*, *131*, 1–11. https://doi.org/10.1016/j.neuroscience.2004.09.066

Skaggs, W. E., McNaughton, B. L., & Gothard, K. M. (1993). An information-theoretic approach to deciphering the hippocampal code. In S. J. Hanson, J. D. Cowan, & C. L. Giles (Eds.), *Advances in neural information processing systems* (Vol. 5, pp. 1030–1037). Cambridge, Massachusetts: MIT Press.

Steffenach, H.-A., Witter, M., Moser, M.-B., & Moser, E. I. (2005). Spatial memory in the rat requires the dorsolateral band of the entorhinal cortex. *Neuron*, *45*(2), 301–313. https://doi.org/10.1016/j.neuron.2004.12.044

Steward, O. (1976). Topographic organization of the projections from the entorhinal area to the hippocampal formation of the rat. *The Journal of Comparative Neurology*, *167*(3), 285–314. https://doi.org/10.1002/cne.901670303

Stranahan, A. M., & Mattson, M. P. (2010). Selective vulnerability of neurons in layer II of the entorhinal cortex during aging and Alzheimer's disease. *Neural Plasticity*, *2010*, 108190. https://doi.org/10.1155/2010/108190

Tamamaki, N., & Nojyo, Y. (1995). Preservation of topography in the connections between the subiculum, field CA1, and the entorhinal cortex in rats. *The Journal of Comparative Neurology*, *353*(3), 379–390. https://doi.org/10.1002/cne.903530306

Tennant, S. A., Fischer, L., Garden, D. L. F., Gerlei, K. Z., Martinez-Gonzalez, C., McClure, C., Wood, E.R., & Nolan, M. F. (2018). Stellate cells in the medial entorhinal cortex are required for spatial learning. *Cell Reports*, *22*(5), 1313–1324. https://doi.org/10.1016/j.celrep.2018.01.005

Tsao, A., Moser, M.-B., & Moser, E. I. (2013). Traces of experience in the lateral entorhinal cortex. *Current Biology: CB*, *23*(5), 399–405. https://doi.org/10.1016/j.cub.2013.01.036

Tsao, A., Sugar, J., Lu, L., Wang, C., Knierim, J. J., Moser, M.-B., & Moser, E. I. (2018). Integrating time from experience in the lateral entorhinal cortex. *Nature*, *561*(7721), 57–62. https://doi.org/10.1038/s41586-018-0459-6

Van Cauter, T., Camon, J., Alvernhe, A., Elduayen, C., Sargolini, F., & Save, E. (2013). Distinct roles of medial and lateral entorhinal cortex in spatial cognition. *Cerebral Cortex*, *23*(2), 451–459. https://doi.org/10.1093/cercor/bhs033

Vandrey, B., Garden, D. L. F., Ambrozova, V., McClure, C., Nolan, M. F., & Ainge, J. A. (2020). Fan cells in layer 2 of the lateral entorhinal cortex

are critical for episodic-like memory. *Current Biology: CB*, *30*(1), 169–175.e5. https://doi.org/10.1016/j.cub.2019.11.027

van Strien, N. M., Cappaert, N. L. M., & Witter, M. P. (2009). The anatomy of memory: An interactive overview of the parahippocampal-hippocampal network. *Nature Reviews. Neuroscience*, *10*(4), 272–282. https://doi.org/10.1038/nrn2614

Wang, C., Chen, X., Lee, H., Deshmukh, S. S., Yoganarasimha, D., Savelli, F., & Knierim, J. J. (2018). Egocentric coding of external items in the lateral entorhinal cortex. *Science*, *362*(6417), 945–949. https://doi.org/10.1126/science.aau4940

Wan, H., Aggleton, J. P., & Brown, M. W. (1999). Different contributions of the hippocampus and perirhinal cortex to recognition memory. *The Journal of Neuroscience*, *19*(3), 1142–1148. https://www.ncbi.nlm.nih.gov/pubmed/9920675

Warburton, E. C., & Brown, M. W. (2010). Findings from animals concerning when interactions between perirhinal cortex, hippocampus and medial prefrontal cortex are necessary for recognition memory. *Neuropsychologia*, *48*(8), 2262–2272. https://doi.org/10.1016/j.neuropsychologia.2009.12.022

Wilson, D. I. G., Langston, R. F., Schlesiger, M. I., Wagner, M., Watanabe, S., & Ainge, J. A. (2013). Lateral entorhinal cortex is critical for novel object-context recognition. *Hippocampus*, *23*(5), 352–366. https://doi.org/10.1002/hipo.22095

Wilson, D. I. G., Watanabe, S., Milner, H., & Ainge, J. A. (2013). Lateral entorhinal cortex is necessary for associative but not nonassociative recognition memory. *Hippocampus*, *23*(12), 1280–1290. https://doi.org/10.1002/hipo.22165

Winters, B. D., Forwood, S. E., Cowell, R. A., Saksida, L. M., & Bussey, T. J. (2004). Double dissociation between the effects of peri-postrhinal cortex and hippocampal lesions on tests of object recognition and spatial memory: Heterogeneity of function within the temporal lobe. *Journal of Neuroscience*, *24*(26), 5901–5908.

Witter, M. P., Wouterlood, F. G., & Naber, P. A. (2000). *Anatomical organization of the parahippocampal-hippocampal network* (Vol. 911, pp. 1–24). *Annals of the New York Academy of Sciences*.

SUPPORTING INFORMATION

Additional supporting information may be found online in the Supporting Information section at the end of this article.

How to cite this article: Vandrey B, Duncan S, Ainge JA. Object and object-memory representations across the proximodistal axis of CA1. *Hippocampus*. 2021;31:881–896. https://doi.org/10.1002/hipo.23331